ELSEVIER

TiO$_2$–CuO three-dimensional heterostructure obtained using short time photochemical deposition of copper oxide inside a porous nanocrystalline TiO$_2$ layer

E. Vigil [a,b,*], F.A. Fernández-Lima [c], J.A. Ayllón [d], E. Pedrero [b], I. Zumeta [b], B. González [b], L. Curbelo [a], H.D. Fonseca Filho [e], M.E.H. Maia da Costa [e], C. Domingo [f], M. Behar [g], F.C. Zawislak [g]

[a] *Facultad de Física, Univ. de la Habana, Colina Universitaria, C. Habana 10400, Cuba*
[b] *Inst. Ciencia y Tecnología de Materiales, Zapata casi esq. a Calle G, Univ. de La Habana, Cuba*
[c] *Inst. Superior de Tecnologías y Ciencias Aplicadas, Avenida Salvador Allende esq Luaces, s/n, C. Habana 10600, Cuba*
[d] *Universitat Autónoma de Barcelona, 08290 Cerdanyola del Valles, Spain*
[e] *Dept. de Física, Pontifícia Univ. Católica do Río de Janeir, Rua Marqués de Saõ Vicente, 225-Gávea, 22452-970, Río de Janeiro, RJ, Brazil*
[f] *Institut de Ciencia de Materiales de Barcelona, CSIC, 08290 Cerdanyola del Vallés, Spain*
[g] *Dept. de Física, Univ. Federal do Rio Grande do Sul, Brazil*

Abstract

Solid inorganic three-dimensional nanocrystalline heterostructures are being studied lately, particularly, regarding photovoltaic structures and as a possible alternative to a solid dye sensitized solar cell (DSSC). Unbiased electron injection from copper species to porous nanocrystalline TiO$_2$ has been reported recently for TiO$_2$–copper oxide photoelectrodes immersed in an aqueous electrolyte; demonstrating that relative position of band edges of these two nanocrystalline semiconductor oxides under illumination encourages pursuing a three-dimensional nanocrystalline TiO$_2$–Cu$_x$O heterostructure. Here, copper oxide deposition inside a porous nanocrystalline TiO$_2$ film using a more efficient photochemical deposition technique is studied further and described. Samples obtained using UV-radiation incident through the conducting glass substrate and samples radiated from the TiO$_2$ side are prepared and studied. Relative concentration of copper species in the TiO$_2$ surface layer is analyzed using Rutherford backscattering spectrometry (RBS). Comparison of both sample types gives an idea of copper species distribution along the incident direction of the reaction-provoking UV-radiation. XPS analysis of TiO$_2$ surface was used to determine oxidation state of copper species present, as well as, their relative proportions. AFM images and roughness analysis clearly show the effect of the dependence of UV-radiation absorption with penetration distance. Finally, the photocurrent dependence with time corresponding to both sample types is studied, compared and explained.
© 2007 Elsevier Inc. All rights reserved.

Keywords: Heterostructure; Nanocrystalline; Photochemical deposition; Copper oxide; Titanium dioxide

1. Introduction

Great interest exists toward solid inorganic three-dimensional nanocrystalline heterostructures, in particular for solar energy conversion devices [1–3]. Recently, unbiased electron injection from copper species to a porous nanocrystalline TiO$_2$ film for TiO$_2$–copper oxide photoelectrodes immersed in an aqueous electrolyte has been

---

* Corresponding author. Present address: Facultad de Física – Inst. Ciencia y Tecnología de Materiales, Univ. de La Habana, Zapata casi esq. a Calle G, Ciudad Habana 10400, Cuba. Tel.: +537 878 89 58; fax: +537 878 34 71.
E-mail address: evigil@fisica.uh.cu (E. Vigil).

reported [4]. Electron injection demonstrates that relative position of band edges under illumination of these two nanocrystalline semiconductor oxides encourages pursuing a three-dimensional nanocrystalline TiO_2–Cu_xO interface for photovoltaic applications. Copper oxides are suitable for these applications because they are abundant, readily available, low-cost and non-toxic. These characteristics plus their absorption spectra that cover a wide range of the solar spectrum, make these oxides good candidates for a three-dimensional nanocrystalline heterostructure with porous nanocrystalline TiO_2. Both, Cu_2O and CuO, show p-type conductivity. CuO is grey-black in color with a monoclinic crystal structure and a band gap of 1.2–1.5 eV [5]. Cu_2O has a reddish appearance, a cubic crystal structure and a direct band gap of about 2.0–2.2 eV [6,7]. According to their band gap values that determine their absorption edges, CuO absorbs a wider solar spectrum range.

Here, we study further copper oxide deposition into porous nanocrystalline TiO_2 using a new photochemical deposition technique that allows relatively short deposition times and which is described. This technique is quite simple. Samples obtained using UV-radiation incident through the conducting glass substrate and samples radiated from the TiO_2 side are prepared and studied. It is expected that results should be better, the greater the coverage of the TiO_2 real surface (it includes internal surface due to porosity) and the smaller the deposit thickness (smaller than the electron recombination length in the copper oxide). For sample characterization SEM, X-ray diffraction and optical transmission are performed. Using Rutherford backscattering spectrometry (RBS) copper species relative areal densities for the TiO_2 surface layer are analyzed. XPS analysis of TiO_2 surface was used to determine oxidation state of copper species present, as well as, their relative proportions. For morphological characterization, topography and roughness of the structures have been studied using atomic force microscopy (AFM). Finally, photocurrent dependences with time corresponding to two-electrode photochemical cells with both sample types as photoelectrodes, are studied, compared and explained.

2. Experimental

2.1. Sample preparation

TiO_2 porous films were produced using doctor's blade technique as described by Smestad [8]. Indium–tin-oxide (ITO) covered glass with $15\,\Omega^2$ sheet resistivity was employed as substrate. After films were dried at room temperature, they were annealed at 400 °C during 1 h. Layers 4–5 μm thick were obtained. An aqueous solution of copper(II) formate ($(HCO_2)_2Cu$, Aldrich) was used as precursor to cover the TiO_2 porous surface. Prior to irradiation, samples were immersed for 24 h in a 40 mM $(HCO_2)_2Cu$ aqueous solution to ensure pore filling [4].

Samples were irradiated using a high-pressure Hg lamp. Samples were positioned so that radiation intensity received was 4 mW/cm^2 at $\lambda \approx 350$ nm. This intensity was measured with a calibrated photodiode. When the porous nanocrystalline TiO_2 is brought into contact with the solution and irradiated, the interaction of UV-light with TiO_2 produces electron–hole pairs. Holes oxidant capacity is responsible for formate oxidation and electrons reduce Cu(II) to Cu(0). Metallic copper is not stable in these experimental conditions being reoxidized to Cu(I) and/or Cu(II) [9,10].

For irradiation, each TiO_2 layer was placed against an optical glass slide in an up-right position with their lower part immersed in a 40 mM $(HCO_2)_2Cu$ precursor solution (see Fig. 1). Due to capillarity, the solution rises and fills pores. This ensures continued pore filling due to capillary flow during irradiation that causes deposition and also water evaporation. With this set-up, two types of samples were obtained: sample type IT, UV-irradiated through the TiO_2 and sample type IS, UV-irradiated through the substrate. A higher intensity UV-light source and continuous capillary flow of precursor solution during irradiation time, allowed reducing irradiation time of several hours [4] to less than 10 min. After irradiation, samples were heat treated for 1 h at 400 °C and then washed with deionized water. Temperature was chosen in order to oxidize Cu(I) to Cu(II) since CuO has a wider spectral range than Cu_2O. It is expected that oxidation is guaranteed at this temperature according to reports from different authors [11–15].

2.2. Samples characterization

Transmission spectra were obtained using an HP8453 spectrometer to have a relative indication of copper oxide
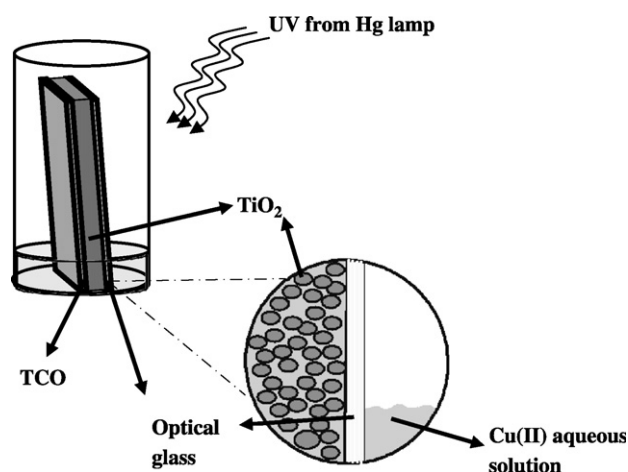
Fig. 1. Experimental set-up scheme for photochemical deposition irradiating through TiO_2. TiO_2 layers were placed against an optical glass slide in an up-right position during UV-irradiation. The lower part of the layer is immersed in the precursor solution; which rises and fills pores due to capillarity.

deposited on the TiO$_2$. Measurements were performed using a conducting substrate as blank.

For SEM analysis a scanning electron microscope Hitachi S-570, 10–30 kV, was used and samples were gold covered. Porous TiO$_2$ thickness was characterized from SEM photos of fractured layer edges at 45°. Thickness is in the range of 4–5 μm.

X-ray diffraction was performed with a Rigaku Rotaflex Ru-200 B apparatus. Cu Kα radiation ($\lambda = 0.154056$ nm) was used for all X-ray diffraction experiments.

The ion-beam analysis were made using a 3 MV TANDETRON accelerator of the Institute of Physics, Federal University of Rio Grande do Sul, Brazil. Rutherford Backscattering Spectrometry (RBS) was used to measure the Ti, Cu and O content by means of a 2.8 MeV ^{4}He$^+$ beam. A surface barrier detector located at 165° with respect to the incident beam was used to detect the backscattered ions. The overall resolution of the detector plus the associated electronics was better than 13 keV (FWHM). RBS spectra were analyzed using the RUMP program [16]. We were able to determine areal density and stoichiometry from the fit obtained using Rump algorithm.

The AFM measurements were performed with a commercial microscope (Nanoscope III, Digital Instruments) operated in tapping mode for topography analysis. All the experiments were performed at room temperature and air relative humidity was kept constant at 40%. The image resolution was set to 65,536 pixels per image (256 × 256). Root mean square roughness was measured for several scanned areas ranging from 1 × 1 to 50 × 50 μm^2.

XPS spectra were obtained using a Mg Kα X-ray source and a hemispheric analyzer CLAM4 from VG Instruments. The angle between sample surface and electron energy analyzer axis was 60°. Binding energies (BE) were calculated using C 1s peak (284.5 eV) as an internal reference. After subtracting a nonlinear background, each spectrum was resolved into individual component bands of a convoluted Gaussian–Lorentzian (20%) line shape.

A two-electrode photoelectrochemical cell was used for photocurrent measurements which has been previously described [17]. The cell uses a thin liquid electrolyte layer and it is based on the capillary rise of the electrolyte. It has a Pt counter-electrode and its geometry allows direct incidence of radiation on the photoelectrode. The electrolyte was a 0.5 mM Na$_2$SO$_4$ aqueous solution. A 100 W halogen lamp was used and radiation intensity on the sample was approximately one sun. The memory capacity of a KEITHLEY 2001 multimeter was adequate for measuring photocurrent dependence with time when the sample is illuminated and when the light is shut off.

3. Results and discussion

Samples surfaces were observed using SEM. Differences are hardly visible between samples that were UV-irradiated through the glass substrate during photochemical deposition reaction (sample type IS) and bare TiO$_2$ samples. This shows that nanocrystals larger than original TiO$_2$ ones, are not formed in this case. In Fig. 2a and b, surface of sample UV-irradiated through the TiO$_2$ surface (sample type IT) is shown. Deposited crystals larger than TiO$_2$ film nanocrystals were visible in some points (see Fig. 2a). Most probably, this could be avoided in future experiments. Comparison of nanocrystalline structure of samples surface before and after photochemical deposition shows little difference (Fig. 2b and c). It seems that copper oxide deposition provokes some necking among smaller nanocrystals.

The logarithm of the inverse of optical transmission is shown in Fig. 3. Light which is not transmitted is either absorbed or scattered. TiO$_2$ absorption edge appears for photon energies higher than 3.0 eV ($E_g = 3.0$ eV for rutile and $E_g = 3.2$ eV for anatase). Therefore, the dependence shown for TiO$_2$ in Fig. 3 is due to scattered light. The difference between curves shown for TiO$_2$ deposited samples and the one corresponding to bare TiO$_2$ is explained by copper species optical absorption. This is also evident to the naked eye since samples turn brownish after
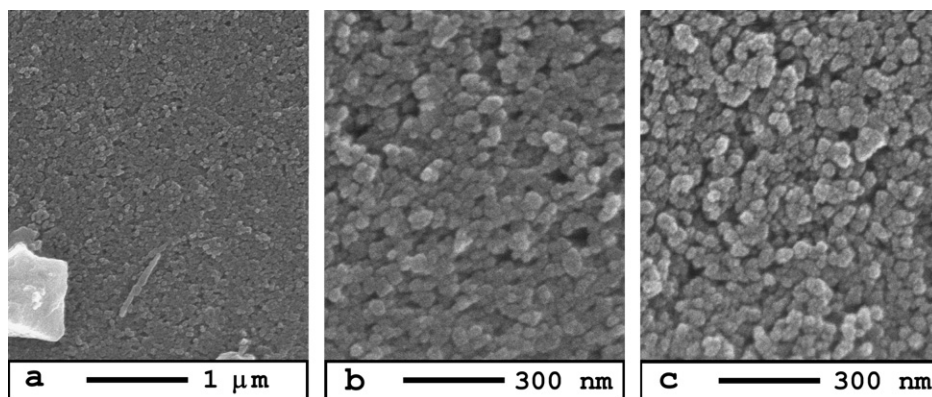
Fig. 2. (a) Surface of sample type IT (irradiated through the TiO$_2$ surface during photochemical deposition reaction) where some undesired larger particles are observed. (b) Same sample showing nanocrystalline structure after photochemical reaction. (c) Surface of TiO$_2$ film before photochemical deposition is shown for comparison with (b).
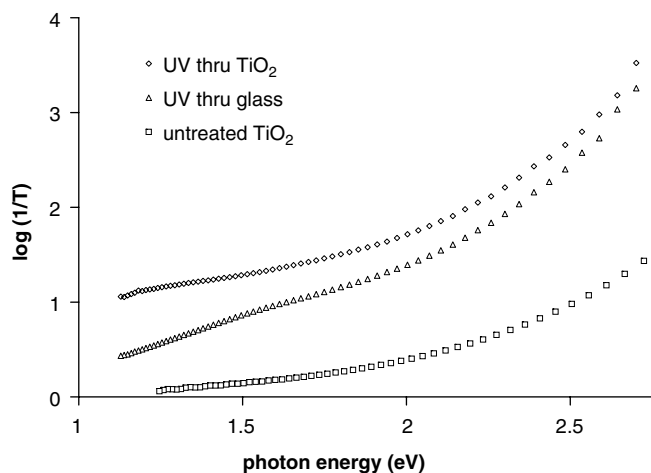
Fig. 3. Light absorption and/or scattering corresponding to samples type IT, (UV-irradiated through the TiO$_2$ during photochemical deposition), samples type IS (UV-irradiated through the glass substrate) and TiO$_2$ before deposition.

Fig. 4. X-ray diffraction spectra (Cu Kα radiation, $\lambda = 0.154056$ nm) corresponding to: (a) TiO$_2$ film before photochemical deposition, (b) sample type IT, UV-irradiated through the TiO$_2$ during photochemical deposition and (c) sample type IS, UV-irradiated through the glass substrate.

Table 1
RBS simulation result for IT, IS and TiO$_2$ samples

Sample	Thickness(10^{15} atom/cm^2)	StoichiometryTi:O:Cu
IT	2600	1:2:(0.4 → 0.03)
	$+\infty$	1:2:0.03
IS	$+\infty$	1:2:0.02
TiO$_2$	$+\infty$	1:2:0

Note: $+\infty$ means that the thickness can not be determined because the TiO$_2$ layer is too thick for RBS ($>20,000 \times 10^{15}$ atom/cm^2).

photochemical deposition. Samples irradiated through the TiO$_2$ have stronger light absorption (darker) than those irradiated through the substrate. This shows that the conducting glass absorbs part of the radiation intensity during photochemical deposition reaction, i.e., reaction-provoking UV-radiation intensity is smaller for this sample type (IS).

Fig. 4 shows X-ray diffraction spectra for samples type IT and IS UV-irradiated during photochemical deposition reaction through the TiO$_2$ and glass substrate, respectively. For both sample types (Fig. 4a and b), X-ray diffraction patterns only show peaks corresponding to anatase and rutile, as well as, In$_2$O$_3$, i.e., ITO conducting layer (In$_2$O$_3$:Sn). No lines corresponding to Cu, CuO or Cu$_2$O appear. RBS and XPS results that follow show that Cu to Ti atoms proportion is high enough for lines to be present if copper species had deposited as crystals. Therefore, one has to conclude that copper species do not tend to crystallize. They either adhere to TiO$_2$ and/or form amorphous particles.

The reported concentrations in Table 1 have been obtained from the simulation of the RBS spectra (see Fig. 5). Concentrations correspond to a thin top layer (a few microns) of the covered TiO$_2$ according to the small penetration depth of the incident beam. Samples are irradiated during growth through different sample faces, but RBS is always performed on the TiO$_2$ surface.

The RBS simulation gives the sample stoichiometry as a function of distance from the surface. In order to give these penetration values, it is necessary to know the sample mass density, which is not known. Therefore, areal density, which is proportional to penetration, is reported in Table 1. For example, for pure non-porous anatase, $20,000 \times 10^{15}$ atoms/cm^2 areal density corresponds to 2.3 µm penetration depth. Samples IS and TiO$_2$ show a constant stoichiometry over the first few penetrated microns. In Table 1 this penetration (given as areal density) was consider as infinite

for the RBS analysis. Moreover, sample IT shows a different stoichiometry as a function of depth, i.e., the number of Cu atoms decreases from 40 to 3 atoms per 100 Ti atoms in the first 2600×10^{15} atom/cm^2, and it remains at 3 Cu atoms per 100 Ti atoms over the rest of possible penetration. The RBS simulation cannot determine the Cu composition depth profile due to the large roughness of the IT sample surface. For all the samples (i.e., IT, IS and TiO$_2$) a Ti:O stoichiometry of 1:2 was obtained.

As observed from Table 1, copper concentration in the surface for samples IS, UV-irradiated through the conducting glass substrate, is 20 times smaller than for samples IT, irradiated through the substrate. It has to be taken into consideration that RBS only includes a thin top layer.
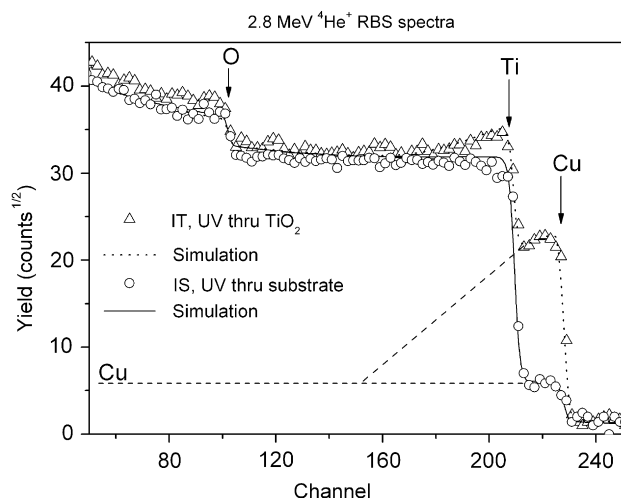
Fig. 5. 2.8 MeV ^{4}He$^+$ RBS spectra and simulation for IT and IS samples. Arrows indicate the starting position of Ti, O and Cu signals. The dash line at the bottom represents the Cu contribution to the spectra. Notice the higher contribution of Cu atoms at the surface (starting position of the Cu signal) in the IT sample.

The exponential decay of UV-radiation intensity with distance according to Lambert–Beer law must cause surface copper concentration for samples irradiated through the conducting glass substrate to be considerably less. For samples IT, UV-irradiated through the TiO$_2$, the surface must have the highest concentration while for samples IS, the surface must have the smallest concentration. This last one should be smaller than any concentration in sample type IT due to UV-absorption by the conducting glass. The Cu composition values at the surface for sample IT calculated by the RBS simulation (Table 1) could be over-estimated due to contribution from crystals on the surface (see Figs. 2a and 6a). Therefore, one can conclude that concentration must change less than 20 times from surface to bottom.

Table 2
Elemental composition (in atomic percent) determined from XPS analysis

Element	Samples IT (UV-irradiated through TiO$_2$)	Samples IS (UV-irradiated through substrate)
Ti	22.37%	25.9%
O	67.89%	70.6%
Cu	6.3% Cu(0) + 3.4% Cu(II)	3.4% Cu(0)
Ti:O:Cu	1:3.03:0.43	1:2.72:0.13

XPS analysis was used to determine oxidation state of copper species present, as well as, their relative proportions (see Fig. 6).
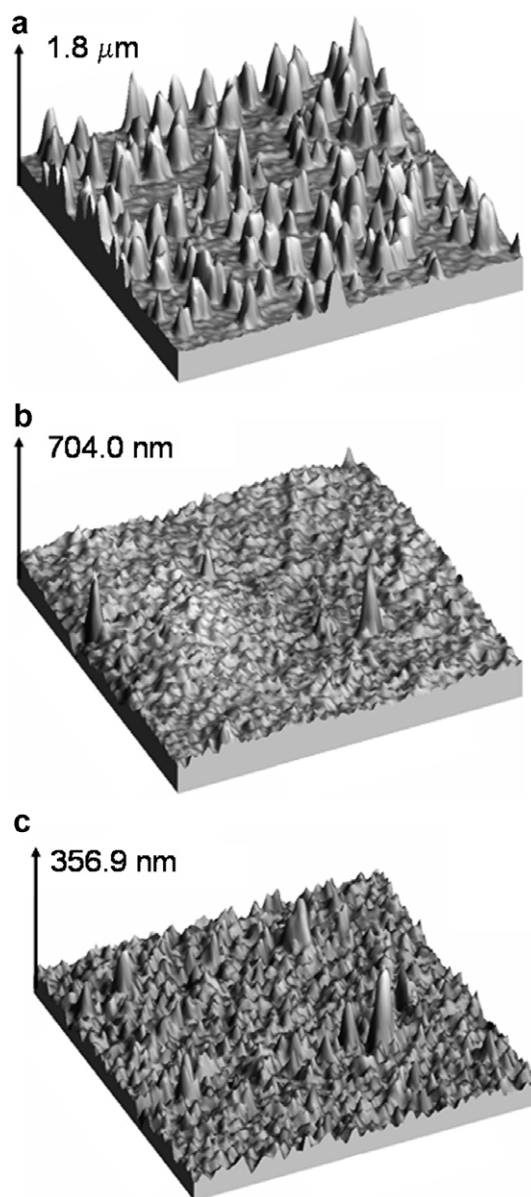
Fig. 7. AFM images corresponding to: (a) sample type IT (UV-irradiated through TiO$_2$ during photochemical deposition), (b) sample type IS (UV-irradiated through the glass substrate) and (c) TiO$_2$ samples before photochemical deposition (scanned area is 30×30 μm^2 for all samples).
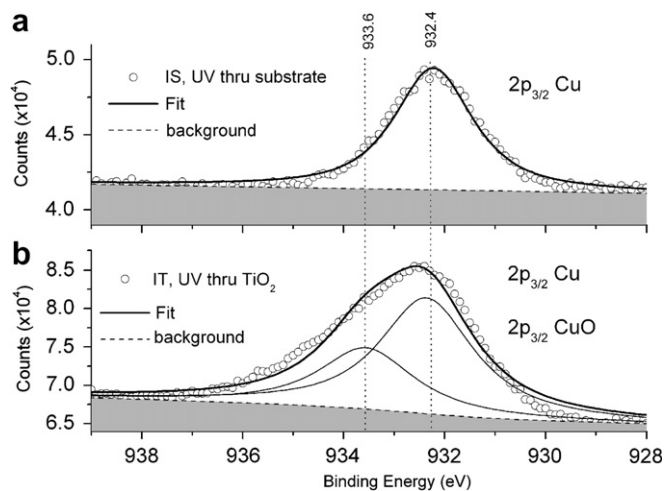
Fig. 6. Curve-fitted XPS spectra of sample types IS (top) and IT (bottom). Notice the 2p$_{3/2}$ Cu and CuO BE lines at 932.4 and 933.6 eV, respectively.

In Table 2 the relative elemental composition for IT and IS samples is presented. The atomic sensitivity factors were considered. XPS analysis gives a relative atomic concentration Ti:Cu equal to 1:0.43 for sample IT and 1:0.13 for sample IS. This is somewhat different from results given by RBS analysis (see Table 1, Ti:Cu equals 1:0.3 for sample IT and 1:0.2 for sample IS). This difference can be explained by XPS smaller depth sensitivity (only the first monolayers are analyzed) plus possible influence of deposits on sample IT surface. The higher oxygen concentrations could be related to OH's on the surface. Since RBS has a higher depth sensitivity (few microns) compare to XPS (few monolayers), RBS gives a better average value for the overall composition.

Two BE lines are observed in the XPS spectra shown in Fig. 6: BE lines at 932.4 and 933.6 eV corresponding to the $2p_{3/2}$ Cu and CuO signals, respectively. Cu(0) is present and Cu_2O is absent in both IT and IS samples. These results also indicate that only in IT samples Cu(II) from CuO was observed and that Cu(0) predominates over Cu(II) in these IT samples (see Table 2). It needs further analysis to explain why Cu(0) did not oxidize to Cu(I) and/or Cu(II) [9,10]; at least on samples surface as analyzed by XPS.

Topography and roughness of the structures have been studied using atomic force microscopy (AFM) for samples morphological characterization. Images corresponding to scanning area of $30 \times 30\ \mu m^2$ are shown in Fig. 7.

In the case of samples IT, deposits exist on the surface of the sample but this does not occur for samples irradiated through the substrate. Deposits on the surface of samples IT contribute to explain the greater concentration of copper species of samples IT found from RBS results.

Samples roughness was calculated from AFM images for different scan lengths (see Table 3). Samples obtained UV-irradiating from the substrate side have practically the same roughness as untreated samples. The increased roughness of samples obtained UV-irradiating from the TiO$_2$ side can be explained by deposits formed on the surface (see Fig. 2a and Fig. 7a).

Table 3
Sample roughness calculated from AFM images

Sample	Roughness (nm)				
Scanned area (μm^2)	1×1	5×5	10×10	30×30	50×50
Sample IT, UV through TiO$_2$	20.6	21.8	190.0	208.2	237.0
Sample IS, UV through substrate	15.4	19.4	21.6	38.8	55.9
TiO$_2$	14.0	20.4	23.3	31.2	63.8

According to Fig. 8 a, samples IT irradiated through the TiO$_2$ during photochemical deposition show photocurrent in the direction produced by electrons moving toward the TiO$_2$ indicating electron injection from CuO to the TiO$_2$, i.e., the photoelectrode behaves as n-type. The photocurrent in the steady state is less than one fifth of initial photocurrent (see Fig. 8a). Samples IS irradiated through the substrate show photocurrent in the opposite direction and it goes to zero rather fast (see Fig. 8b). For samples IS UV-irradiated through the substrate, CuO must have deposited in contact with the conducting oxide explaining the photocurrent direction, i.e., electrons moving to the electrolyte, as in a p-type photoelectrode.

Time dependence for photocurrent decay in samples type IT shows three different regions. First, the photocurrent decreases with a 40 s time constant, then for $20 < t < 80$ s it decreases with a 200 s time constant and finally, photocurrent decreases very slowly with a time constant of 3000 s. The final slow decay could be due to photoelectrode degradation. Further experimentation is necessary to explain the different electron recombination mechanisms that cause photocurrent decay.

4. Conclusions

CuO is formed into porous nanocrystalline TiO$_2$ using a more efficient photochemical deposition technique. Samples are UV-irradiated with a high-pressure Hg lamp during 9 min followed by heat treatment. XPS analysis show that CuO as well as Cu(0) appear in nanocrystalline TiO$_2$
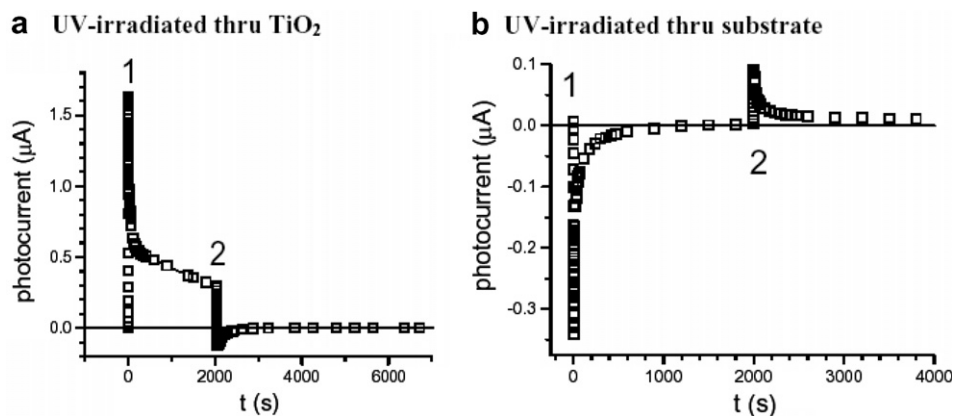
Fig. 8. Photocurrent transient behavior when illuminated. In 1 photoelectrode is illuminated and in 2 light is shut off. (a) Samples IT irradiated through the TiO$_2$ during photochemical deposition. (b) Samples IS irradiated through the conducting glass substrate during photochemical deposition.

surface layer indicating that Cu(0) does not oxidize completely. RBS analysis shows that Cu species concentration depends on UV intensity distribution inside the porous TiO_2 during photochemical deposition. According to RBS results it is concluded that concentration changes less than 20 times from sample surface to bottom. SEM and AFM analysis show that deposits form on the surface of TiO_2 when samples are UV-irradiated through the TiO_2 but not when samples are irradiated through the conducting glass substrate. There is practically no change in surface roughness in the last case when compared to bare TiO_2 samples. Electron injection from CuO to TiO_2 occurs when samples IT, UV-irradiated for deposition through the TiO_2, are used as photoelectrodes using an aqueous electrolyte.

Acknowledgments

References

[1] K. Ernst, A. Belaidi, R. Könenkamp, Semicond. Sci. Technol. 18 (2003) 475.

[2] M. Nanu, J. Schoonman, A. Goossens, Adv. Mater. 16 (2004) 453.

[3] I. Gur, N.A. Fromer, M.L. Geier, A.P. Alivisatos, Science 310 (2005) 462.

[4] E. Vigil, B. Gonzalez, I. Zumeta, C. Domingo, X. Domenech, J.A. Ayllon, Thin Solid Films 489 (2005) 50.

[5] F. Marabelli, G.B. Parraviciny, F. Salghetti-Drioli, Phys. Rev. B 52 (1995) 1433.

[6] T.D. Golden, M.G. Shumsky, Y. Zhou, R.A. VanderWerf, R.A. Van Leeuwen, J.A. Switzer, Chem. Mater. 8 (1996) 2499.

[7] S.C. Ray, Solar Energy Mater. Solar Cells 68 (2001) 307.

[8] G.P. Smestad, Solar Energy Mater. Solar Cells 55 (1998) 157.

[9] N.S. Foster, R.D. Noble, C.A. Koval, Environ. Sci. Technol. 27 (1993) 350.

[10] K. Chiang, R. Amal, T. Tran, Adv. Environ. Res. 6 (2002) 471.

[11] J.F. Pierson, A. Thobor Kech, A. Billard, Appl. Surf. Sci. 210 (2003) 359.

[12] L. Armelao, D. Barreca, M. Bertapelle, G. Bottaro, C. Sada, E. Tondella, Thin Solid Films 442 (2003) 48.

[13] M.T.S. Nair, L. Guerrero, O.L. Arenas, P.K. Nair, Appl. Surf. Sci. 150 (1999) 143.

[14] J.M. Valtierra, S. Calixto, F. Ruiz, Thin Solid Films 460 (2004) 58.

[15] N. Serin, T. Serin, Ş. Horzum, Y. Çelik, Semicond. Sci. Technol. 20 (2005) 398.

[16] L.R. Doolittle, Nucl. Instrum. Meth. B 9 (1985) 344.

[17] I. Zumeta, R. Espinosa, J.A. Ayllón, X. Domènech, R. Rodríguez-Clemente, E. Vigil, Solar Energy Mater. Solar Cells 76 (2003) 15.